Electronic structure and magnetic properties of metallocene multiple-decker sandwich nanowires

C. Morari,[1] H. Allmaier,[2] F. Beiuşeanu,[3] T. Jurcuţ,[3] and L. Chioncel[4,5]

[1]*National Institute for Research and Development of Isotopic and Molecular Technologies, 65-103 Donath, RO-400293 Cluj Napoca, Romania*

[2]*Institute of Theoretical Physics, Graz University of Technology, A-8010 Graz, Austria*

[3]*Department of Physics, University of Oradea, RO-410087 Oradea, Romania*

[4]*Augsburg Center for Innovative Technologies, University of Augsburg, D-86135 Augsburg, Germany*

[5]*Theoretical Physics III, Center for Electronic Correlations and Magnetism, Institute of Physics, University of Augsburg, D-86135 Augsburg, Germany*

(Received 28 July 2011; revised manuscript received 1 December 2011; published 8 February 2012)

We present a study of the electronic and magnetic properties of the multiple-decker sandwich nanowires (*CP*-*M*) composed of cyclopentadienyl (*CP*) rings and 3*d* transition-metal atoms ($M =$ Ti to Ni) using first-principles techniques. We demonstrate using density functional theory that structural relaxation plays an important role in determining the magnetic ground state of the system. Notably, the computed magnetic moment is zero in *CP*-Mn, while in *CP*-V a significant turn-up in magnetic moment is evidenced. Two compounds show a half-metallic ferromagnetic ground state *CP*-Fe/Cr with a gap within the minority/majority spin channel. In order to study the effect of electronic correlations upon the half-metallic ground states in *CP*-Cr, we introduce a simplified three-band Hubbard model which is solved within the variational cluster approach. We discuss the results as a function of size of the reference cluster and the strength of average Coulomb U and exchange J parameters. Our results demonstrate that for the range of studied parameters $U = 2$–4 eV and $J = 0.6$–1.2 eV the half-metallic character is not maintained in the presence of local Coulomb interactions.

DOI: 10.1103/PhysRevB.85.085413 PACS number(s): 71.15.Mb

I. INTRODUCTION

Utilizing the spin degree of freedom of electrons in solid-state electronics has led to the emergence of the rapidly developing field of spintronics.[1] Important electronic applications based on the magnetoresitive effect in two-dimensional heterostructures already exist. Typical devices are magnetic read heads and nonvolatile magnetic random access memories, where the relative alignment of the layer magnetizations causes large variations of the resistance of the structure. This effect is known as giant magnetoresistance[2] and was discovered in FeCr multilayers,[3] in which the magnetization of the layers couples by indirect exchange interactions, mediated by the electrons of the intermediate layer.[4]

There are continuing efforts to improve material fabrications and design devices for layered magnetic structures. With the development of nanotechnology, quantum structures with dimensions of the order of molecular or atomic size become accessible. In this context, first-principles studies of atomic chain structures that can produce high-polarization effects are important. For instance, complete spin polarization in the absence of magnetic field was predicted for several bulk materials in the class of half-metallic ferromagnets.[5,6] The same properties were predicted for organic nanowires, such as $(C_6H_6)_2V$[7] in $(C_5H_5)Fe$[8] multiple-decker nanowires or in transition-metal-doped silicon nanostructures.[9,10] Organic materials, when used as components of spintronic devices, have significant advantages over inorganic ones. First, the spin-orbit and hyperfine interactions are weak,[11] leading to considerably long spin relaxation length and spin lifetime.[12,13] Organic materials are cheap, low weight, mechanically flexible, and chemically inactive; therefore organic spintronics received considerable attention, in particular because the spin-polarized signal can be mediated and controlled in this case by organic molecules.[14]

Metallocene molecules with the general formula $(C_5H_5)_2M$ consist of two cyclopentadienyl anions (*CP*) bound to a metal center. The metal atom is typically a transition-metal element from the middle of the 3*d* row (i.e., Ti, V, Cr, Mn, Fe, Co, Ni) as well as from the column of iron (i.e., Ru and Os). Molecular structures such as CP_2V, CP_2Cr, CP_2Mn, CP_2Fe, CP_2Co, and CP_2Ni have been studied both experimentally[15–19] and theoretically.[20] Studies were also reported on multidecker sandwich clusters based on C_5H_5 ligands such as triple-decker complexes $CP_3Ni_2^+$ and $CP_3Fe_2^+$[21,22] and multiple-decker sandwich complexes of type $TM(CP_2Fe)_{n+1}$ with $TM =$ V, Ti and $n = 1$–3.[23] The lack of individual bonds between the carbon atoms of the *CP* ring and the metal ion makes the *CP* rings rotate freely about the symmetry axis of the molecule. Although the metallocene's equilibrium structure has a D_{5d} symmetry, the D_{5h} has almost the same probability to occur.[24] Within the equilibrium D_{5d} symmetry, *d* orbitals are split into a d_{z^2} and two sets of doubly degenerate orbitals $d_{xy}/d_{x^2-y^2}$ and d_{xz}/d_{yz}.

The electronic structure calculations based on density functional theory predict for some metallocene wires a half-metallic ferromagnetic ground state,[8,25] stimulating further the search for such candidate materials for spintronic applications.[7,8,25–28] For all transition-metal elements the metallocene wires share the same shape depicted in Fig. 1.

It is expected that the *p*-*d* covalent interactions that take place in metallocene wires are essential for the physical and chemical properties of these compounds. Having similar structure, differences in the electronic properties of $(C_5H_5)_2M_2$ can be traced to the different electronic filling of the *d* orbitals that determines different magnetic interactions. As *d* orbitals form relatively narrow bands in which electronic

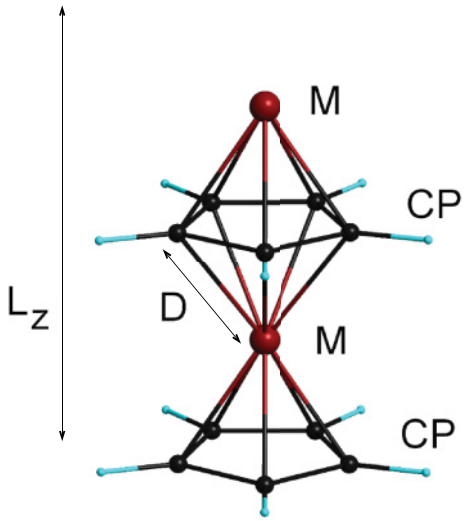

FIG. 1. (Color online) Geometrical structure of the double-decker $(C_5H_5)_2M_2$ sandwich. For the tetragonal unit cell we used fixed values for $L_X = L_Y = 12$ Å while the values of L_Z are transition-metal M dependent. D illustrates the distance between the carbon atom and the transition-metal atom.

correlations are essential, it is natural to raise the question concerning the role of electron-electron interactions in such compounds.

In the present paper we explore the magnetic properties of organometallic multidecker sandwich wires of type $(C_5H_5)M$ where M is a transition metal with atomic numbers ranging from $Z = 22$ (Ti) to $Z = 28$ (Ni). For the interesting case of *CP*-Cr in which half metallicity is predicted by density functional theory–based calculations we formulate a low-energy three-band Hubbard Hamiltonian which is solved using many-body techniques. Our main interest is to understand whether half-metallic magnetism is stable against the electronic correlations in this compound.

II. COMPUTATIONAL DETAILS

We have calculated the electronic and structural properties of the *CP-M* wires within density functional theory (DFT) using the SIESTA code,[29] which employs pseudopotentials and expands the wave functions of valence electrons by linear combinations of numerical atomic orbitals. We have used a double-zeta polarized basis set with an energy cutoff of 30 meV. We have also used a number of 16 k points to model the periodicity along the axis of the wire and a 2×2 grid in the transverse direction. All calculations were performed by using the generalized gradient approximation to the exchange and correlation functional, as parameterized by Perdew, Burke, and Ernzerhof.[30] In order to investigate the magnetism in these compounds we consider a unit cell as shown in Fig. 1 that would naturally allow us to study the stability of ferromagnetic versus antiferromagnetic states. For all systems, we explicitly performed the calculations to look for the stable ferromagnetic and antiferromagnetic configurations allowing structural relaxation. The atomic coordinates of all atoms in the unit cell and the cell's length were relaxed up to a maximum force of 0.01 eV/Å. The values of magnetic moments where computed by integrating the spin-resolved charge density over "muffin-tin" spheres centered on the metal atoms. The radius of the sphere was taken as 2.25 bohr, representing about 55–60 % of the bond length M-C for all complexes. All the calculations were done using the eclipsed configuration of the wires (i.e., D_{5h} symmetry). In order to study the stability of the wires, we compute the binding energy of the metal and *CP* unit, ΔE, defined as $\Delta E = E_{\text{wire}} - 2(E_{CP} + E_M)$, where the total energy of the atom in the unit cell, E_{wire}, and that of cyclopentane unit, E_{CP}, are computed for the relaxed structures and E_M is the total energy of the metallic atom.

III. ELECTRONIC STRUCTURE

Selected parameters of the relaxed wires are given in Table I. We comment in the following upon the atomic-number

TABLE I. Geometric and magnetic properties of the wires. L_Z is the length of the unit cell, D is the metal-carbon distance (see also Fig. 1). M_0 is the magnetic moment per cell, $M_{1/2}$ are the magnetic moments for the transition-metal atoms. AFM/FM, antiferromagnetic/ferromagnetic; NM, nonmagnetic; HMF, half-metallic ferromagnetic. ΔE is the binding energy of the chain. Experimental data on isolated molecules are indicated for the metal-carbon bond length.

Atom	L_Z (Å)	D (Å)	M_0 (μ_B)	$M_{1/2}$ (μ_B)	Type	ΔE (eV)
Ni ($3d^8 4s^2$)	7.35	2.21 (2.20[a])	0.00	0/0	NM	−6.91
Co ($3d^7 4s^2$)	7.10	2.17 (2.12[b])	0.00	1.31/−1.31	AFM	−11.38
Fe ($3d^6 4s^2$)	6.77	2.10 (2.06[c])	2.00	1.00/1.00	HMF	−11.06
Mn ($3d^5 4s^2$)	6.59	2.08 (2.38[d])	0.00	0/0	NM	−8.38
Cr ($3d^5 4s^1$)	6.90	2.14 (2.17[e])	2.00	1.00/1.00	HMF	−7.98
V ($3d^3 4s^2$)	7.20	2.21 (2.28[f])	3.99	1.70/1.70	FM	−13.73
Ti ($3d^2 4s^2$)	7.52	2.29 (2.36[g])	0.00	1.36/−1.36	AFM	−14.98

[a]Reference 31.
[b]Reference 18.
[c]Reference 32.
[d]References 15 and 33.
[e]Reference 16.
[f]Reference 16.
[g]Reference 34.

dependence of the metal-carbon bond lengths. We found that the metal-carbon bond lengths in the investigated *CP*-*M* wires display a regular trend. Large values are realized for the compounds with extreme atomic numbers (i.e., 2.29 Å in the *CP*-Ti chain and 2.21 Å in *CP*-Ni) while the minimum occurs at the intermediate atomic number (i.e., 2.08 Å in the *CP*-Mn chain). We note that the same trend occurs for the relaxed value of the total length, L_Z. The comparison of the computed carbon-metal bond length shows differences ranging between 0.5% (for *CP*-Ni) and about 3% (for *CP*-V). An important difference occurs for *CP*-Mn (i.e., 15%). We note that for *CP*-Mn we also found a ferromagnetic state which is less stable than the nonmagnetic one (the energy difference is 0.15 eV); for this state the C-Mn bond length is 2.12 Å. This magnitude of the bond length is in agreement with the experimentally reported value determined for a high-spin state (see Ref. 15). The vanishing of magnetic moment in the periodic structure is probably the consequence of the large differences between the geometric structure of the molecule and the corresponding chain.

As one can see in Table I the values for the binding energy ΔE depend on the gradual filling of the d orbitals of the metal atom as was observed previously.[20] The strongest binding energy is realized for *CP*-Ti; further filling the d orbital reduces the strength of binding (i.e., nonbonding states are populated[20]). An almost twice weaker binding energy is obtained for *CP*-Cr (−7.98 eV) in comparison with *Cp*-Ti (−14.98 eV). Increasing the number of d electrons starting from Cr → Mn → Fe → Co the binding energy is increasing again, while at *CP*-Co, the partial filling of the antibonding orbitals stops this trend. A further increase of the electronic population in the antibonding orbitals of nanowires leads to an important reduction of the binding energy as seen for the *CP*-Ni wire.

Total densities of states for the seven wires are given in Fig. 2. Increasing the number of valence electrons from Ti ($Z = 22$) to Fe ($Z = 26$) results in a gradual filling of the d band; therefore the Fermi level is expected to be shifted toward higher energies, in addition to which the magnetic interactions contribute in determining the magnetic ground state. In *CP*-Ti and *CP*-V we found that both ferromagnetic and antiferromagnetic states are possible. For Ti the ground-state AF configuration is lower in energy by 0.34 eV, while for V the ferromagnetic is most stable with an energy difference of about 0.17 eV. *CP*-Mn shows long-range ferromagnetic order for a nonrelaxed structure that disappears in favor of a nonmagnetic ground state in the relaxed case. For all the other compounds a single stable solution has been obtained, for the considered range of parameters and configurations. Two systems were found to be half metallic: *CP*-Cr and *CP*-Fe. For *CP*-Cr the gap is situated in the majority spin DOS and it has a value of 0.48 eV, while for the case of *CP*-Fe the gap occurs in the minority spin DOS with a magnitude of about 0.41 eV.

The DOS projected onto the carbon atoms (not shown) has similar shapes as the total density of states but with a significantly smaller weight. In order to determine the character of the orbitals near Fermi level for the interesting case of half-metallic *CP*-Fe and *CP*-Cr we computed the partial densities of states. In the upper panel of Fig. 3, the results for *CP*-Fe are seen. A significant contribution within the majority spin channel is provided by the degenerate

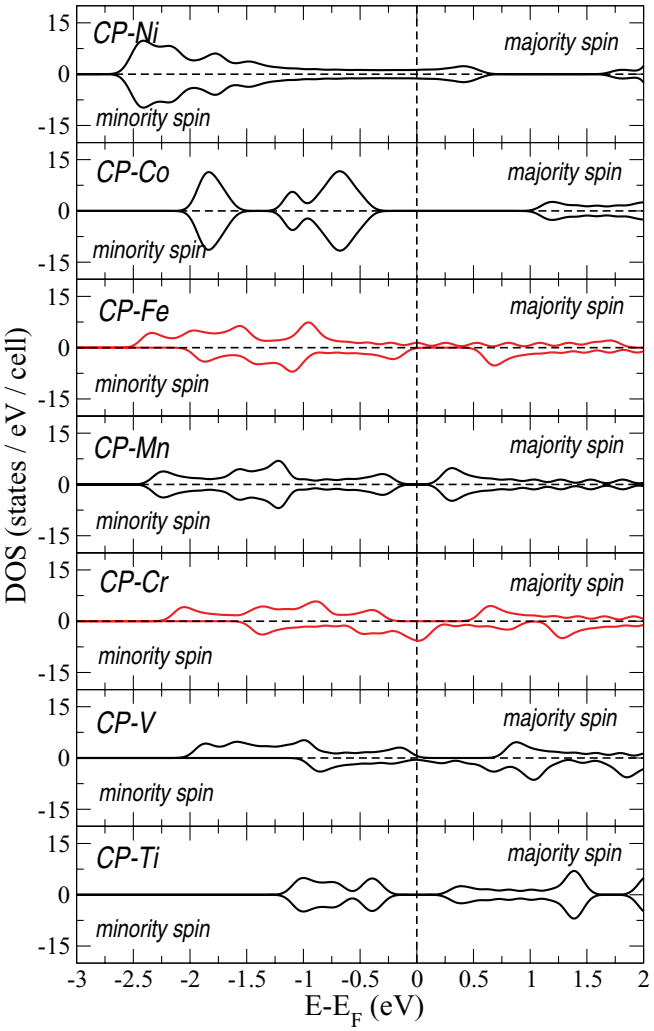

FIG. 2. (Color online) Total DOS for the computed wires. With the red line we show the cases when half metallicity occurs for the *CP*-Fe (minority spin gap) and *CP*-Cr (majority spin gap) sandwiches.

Fe-$3d_{xz}/3d_{yz}$ partially occupied orbitals. The same orbitals are completely empty in the minority spin channel. The other $3d_{z^2}, 3d_{xy}/3d_{x^2-y^2}$ orbitals are completely occupied, so that the gap is realized between the minority spin $3d_{xy}/3d_{x^2-y^2}$ and $3d_{xz}/3d_{yz}$ orbitals. For the case of the majority spin half-metallic *CP*-Cr, the degenerate Cr-$3d_{xz}/3d_{yz}$ are empty in both majority and minority spin channels. Partial occupation is obtained for minority spin $3d_{xy}/3d_{x^2-y^2}$ and $3d_{z^2}$ orbitals, while the same orbitals are completely filled within the majority spin channel. Contrary to *CP*-Fe in *CP*-Cr the gap is realized between the majority spin $3d_{xy}/3d_{x^2-y^2}$ and $3d_{xz}/3d_{yz}$ orbitals. For both half metals, the carbon's p_z orbitals are also present at the Fermi level, however presenting only a weak spectral weight. Note that DOS projected over the p_z orbitals of a carbon atom in the *CP* ring was multiplied by five to facilitate the direct comparison with the total DOS shown in Fig. 2.

The computed magnetic moment per cell for the investigated wires takes values between 0 and 3.99 μ_B, and can be attributed mainly to the transition metals, while the *CP* rings have very weak magnetic moments. The expected monotonic

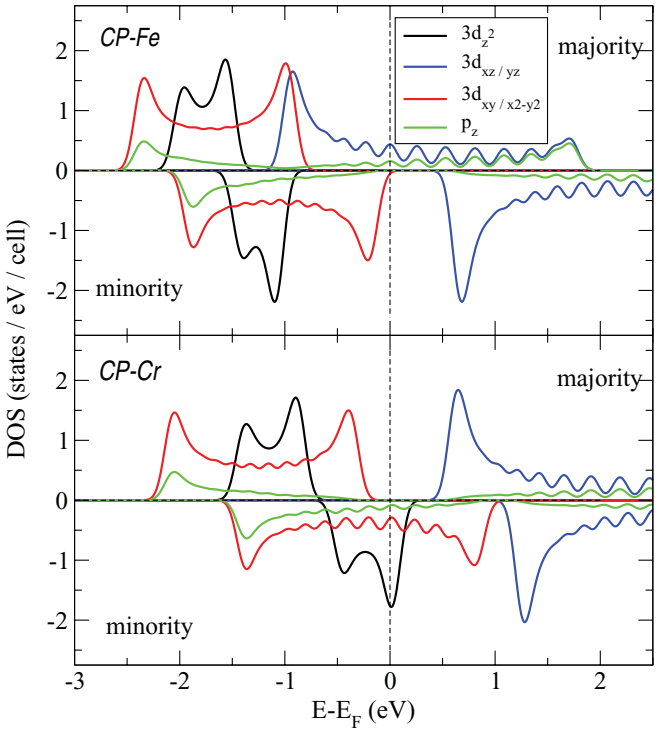

FIG. 3. (Color online) Partial density of states for the half-metallic *CP*-Fe and *CP*-Cr wires. The degenerate M-$3d_{xz}$ and M-$3d_{yz}$ orbitals are represented with blue lines, the red line represents M-$3d_{xz}$ and M-$3d_{x^2-y^2}$ orbitals, and the black line represents the M-$3d_{z^2}$ orbitals (M = Fe, Cr). Finally with the green line we show the sum over the five C-p_z orbitals.

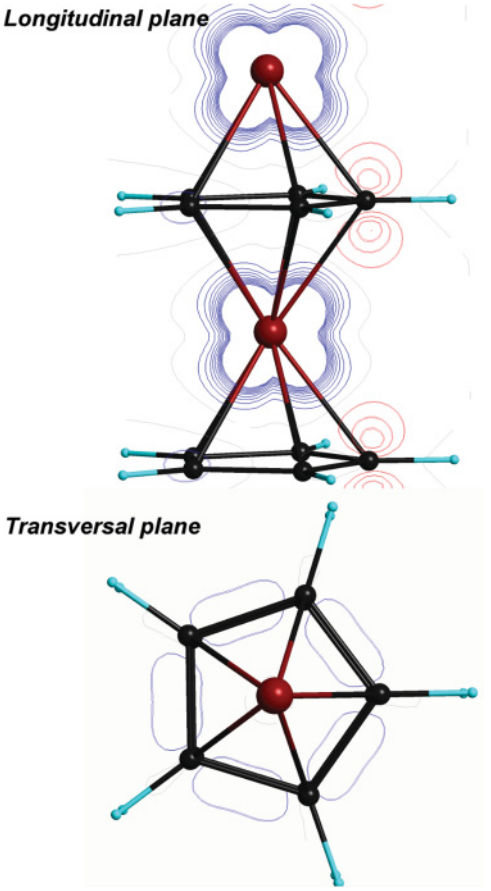

FIG. 4. (Color online) Real-space spin-density contour plots for *CP*-Fe. Majority/minority spin density is represented with blue/red lines. The black lines represent the regions with no difference between up- and down-spin densities. Upper/lower picture presents a side/top view (see text for geometrical details of the contours).

increase of the magnetic moment as a function of d-orbital occupancy can be explained by considering that the metal atom is donating one electron to the *CP* ring, which forms a six-electron π ring. Therefore, $N_{\text{val}} - 1$ electrons rest on the metal and are determinant for its magnetic state, where N_{val} is the number of valence electrons. By using Hund's rule and the transition-metal valence electronic configuration (i.e., $4s$, $3d_{z^2}$, $3d_{xy}/3d_{x^2-y^2}$, and $3d_{yz}/3d_{zx}$, respectively) we can assign a magnetic moment to each wire. We expect therefore the magnetic moments of 0, 2, 4, 2, 0, and 2 μ_B for *CP*-Co, *CP*-Fe, *CP*-Mn, *CP*-Cr, *CP*-V, and *CP*-Ti, respectively. Indeed, the electronic structure calculation provides these results with two remarkable exceptions: *CP*-Mn (0 μ_B instead of 4 μ_B) and *CP*-V (3.99 μ_B instead of 0 μ_B). Note also that *CP*-Ti is an exception from the above discussed Hund's rule as its ground state is antiferromagnetic insulator with moments of ± 1.36. According to our results, the structural relaxation effects determine the departure from the expected behavior in all three compounds: the significant drop/turn-up of the magnetic moment in the *CP*-Mn/V and the weaker reduction of the magnetic moment in the case of *CP*-Ti. We have additionally checked that Mn replacing Cr in the frozen *CP*-Cr structure retains a nonzero magnetic moment (i.e., 2.36 μ_B), with values close to the Cr ones (i.e., 2.0 μ_B). An overall integer magnetic moment on the unit cell (the value M_0 shown in Table I) is obtained for all the compounds.

In Fig. 4 we illustrate with two contour plots the difference between majority and minority real-space spin densities, $n(\mathbf{r})^{\uparrow} - n(\mathbf{r})^{\downarrow}$, for the *CP*-Fe wire. We use two rectangular planes to plot the contours. The first plane has the edges parallel to the z axis and is passing through the metal atoms and one of the carbon atoms in the *CP* ring (top panel Fig. 4). This plane provides us a side view, with respect to the axis of the nanowire. The lower panel of Fig. 4 illustrates the "second" plane that has the edges parallel to the x and y axes and provides a top view of the spin density in the cyclopentane ring. For both spin orientations we use ten equidistant contours and an increment of ± 0.0025 e/bohr^3 for the up-spin/down-spin densities. Note that the spin density on the carbon atom has a maximum value close to 0.0075 e/bohr^3 (i.e., three contour lines). As seen on the contour plot, this maximum value is at least two orders of magnitude lower than the values obtained for the spin densities on the metal site. For Fe the maximum spin density is located around its atomic position and has a value of about 1.2 e/bohr^3 (picture not shown here). In addition for the Fe sites the difference of real-space spin densities has a positive sign (blue contours), while on the carbon sites the difference is negative signaling an antiparallel orientation of a small magnetic moment with respect to Fe magnetic moment.

For *CP*-V a nonzero spin-density contribution is present on the *CP* rings, which makes this material to be an almost half-metallic compound. We also noticed that in the case of *CP*-Co,

the majority spins accumulate on one side of the cyclopentane ring, therefore contributing to the antiferromagnetic properties obtained for *CP*-Co.

IV. MULTIORBITAL HUBBARD MODEL FOR HALF-METALLIC *CP*-Cr CHAIN

A. Model setup

In order to discuss further the magnetic properties of the half-metallic *CP*-Cr metallocene nanowire we supplement the DFT analysis with many-body calculations based on a multiorbital Hubbard model. Such calculations were performed recently for the prototype half-metallic ferromagnet NiMnSb including local[35] and nonlocal correlation[36,37] effects, demonstrating the appearance of significant many-body induced states within the half-metallic gap leading to the disappearance of half metallicity. Our primary goal is to investigate the existence of similar effects in the half-metallic metallocene nanowires, in particular the stability of the half metallicity in the presence of the Coulomb interaction. In the present section we discuss the construction of the low-energy Hamiltonian in a similar way as has been recently performed for NiMnSb,[36,37] CrO_2,[38] or TiN[39] in the framework of the *N*th-order muffin-tin-orbital method. Alternative downfolding schemes can be also formulated within tight-binding approaches.[40,41]

The starting point in the combined electronic structure and many-body calculation is the formulation of the low-energy model Hamiltonian. Specifically, the uncorrelated part of the Hamiltonian is obtained from the downfolding procedure[42,43] within the *N*th-order muffin-tin-orbital (NMTO) method. The NMTO method[42,43] can be used to generate truly minimal basis sets with a massive downfolding technique. Downfolding produces bands with a reduced basis which follow exactly the bands obtained with the full basis set. The truly minimal set of symmetrically orthonormalized NMTOs is a set of Wannier functions. In the construction of the NMTO basis set the active channels are forced to be localized onto the eigenchannel $\mathbf{R}lm$; therefore the NMTO basis set is strongly localized. For *CP*-Cr we choose to downfold (i.e., to integrate out) all orbitals except the Cr-3*d* (xy,x^2-y^2, z^2-1) manifold. At this point is important to mention that the NMTO calculations has been performed considering the structure shown in Fig. 1 with the parameters discussed in Table I. The calculations considered the tetragonal symmetry for the case in which the Cr-3*d* (xy,x^2-y^2) orbitals are nearly degenerate, while in the computation using SIESTA a complete degeneracy is seen as the D_{5h} structural symmetry of the ligand field is considered. This difference turns out not to be essential in considering the many-body effects presented here. Thus, the effective Hamiltonian is confined to the set of three effective orbitals of (xy, x^2-y^2, z^2-1) type in a reduced window of energies. For optimizing the energy window with respect to the orbitals we chose the following expansion points with respect to the Fermi level: $E_v - E_F = 0.31$ eV, -1.05 eV, and -1.59 eV, where the Fermi energy has the absolute value $E_F = -3.44$ eV. In Fig. 5 we show the eigenvalues of the effective Hamiltonian along some high-symmetry directions in comparison with the full orbital basis.

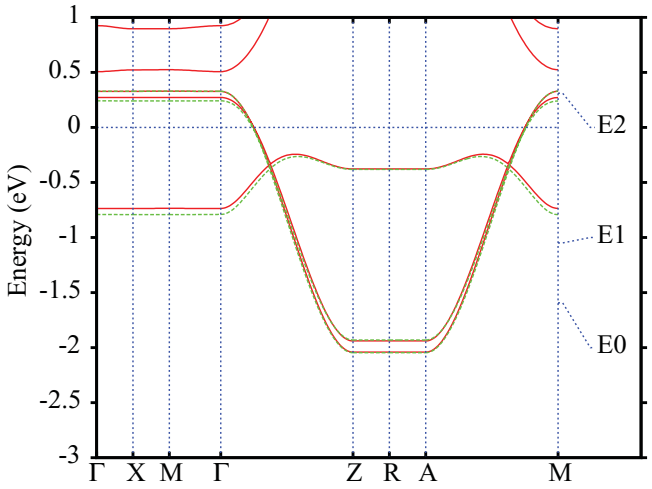

FIG. 5. (Color online) Band structure of *CP*-Cr around Fermi energy obtained with the LDA calculation (red line) for the complete orbital basis set and the NMTO bands obtained after downfolding to the effective xy, x^2-y^2, and z^2-1 orbitals.

Fourier transformation of the orthonormalized NMTO Hamiltonian, $H^{LDA}(\mathbf{k})$, yields on-site energies and hopping integrals,

$$H^{LDA}_{\mathbf{0}m',\mathbf{R}m} \equiv \langle \chi^{\perp}_{\mathbf{0}m'} | \mathcal{H}^{LDA} - \varepsilon_F | \chi^{\perp}_{\mathbf{R}m} \rangle \equiv t^{xyz}_{m',m}, \tag{1}$$

in a Wannier representation, with the orthonormal $|\chi^{\perp}_{\mathbf{R}m}\rangle$-NMTO Wannier functions. m is labeled by the three xy, x^2-y^2, z^2-1 orbitals. In this representation the on-site matrix elements $t^{000}_{m',m}$ are nearly diagonal; a very small nonzero coupling between the x^2-y^2 and z^2-1 orbitals is obtained, which is a consequence of the considered tetragonal symmetry. A set of rotated orbitals has to be introduced such that the local single-particle density matrix is diagonalized. Such a procedure is frequently used[41] and in the present case this leads to a small change in the effective hopping parameters of *CP*-Cr. The on-site and the directional hopping matrix elements within the rotated basis set are given (in units of eV) by

$$t^{000}_{m',m} = \begin{pmatrix} -4.245 & 0 & 0 \\ 0 & -4.287 & 0 \\ 0 & 0 & -3.869 \end{pmatrix},$$
$$t^{00\pm1}_{m',m} = \begin{pmatrix} -0.545 & 0 & 0 \\ 0 & -0.589 & -0.02 \\ 0 & -0.02 & 0.091 \end{pmatrix}. \tag{2}$$

Thus, the noninteracting part of the effective Hamiltonian for *CP*-Cr has the form

$$H_0 = \sum_{\mathbf{R}',\mathbf{R},\{m',m\},\sigma} t^{\mathbf{R}'-\mathbf{R}}_{m',m} c^{\dagger}_{\mathbf{R}'m'\sigma} c_{\mathbf{R}m\sigma} + \text{H.c.} \tag{3}$$

To take into account correlation effects to the noninteracting Hamiltonian in Eq. (3) we add the Hubbard part such that a 3-band "correlated" Hamiltonian is cast in the form

$$H = H_0 + \sum_{\mathbf{R}m} U n_{\mathbf{R}m\uparrow} n_{\mathbf{R}m\downarrow} + \sum_{\mathbf{R},m<m',\sigma,\sigma'} (U' - J\delta_{\sigma,\sigma'}) n_{\mathbf{R}m\sigma} n_{\mathbf{R}m'\sigma'}$$

$$+ \sum_{\mathbf{R},m<m'} J_{mm'} c^{\dagger}_{\mathbf{R}m'\uparrow} c^{\dagger}_{\mathbf{R}m\downarrow} c_{\mathbf{R}m'\downarrow} c^{\dagger}_{\mathbf{R}m\uparrow} + \text{H.c.}$$

$$+ \sum_{\mathbf{R},m<m'} J_{mm'} c^{\dagger}_{\mathbf{R}m'\uparrow} c^{\dagger}_{\mathbf{R}m'\downarrow} c_{\mathbf{R}m\downarrow} c^{\dagger}_{\mathbf{R}m\uparrow} + \text{H.c.}, \quad (4)$$

where H_0 is given by Eq. (3), $n_{\mathbf{R}m\sigma} = c^{\dagger}_{\mathbf{R}m\sigma} c_{\mathbf{R}m\sigma}$ is the number of particle operator, and $c^{\dagger}_{\mathbf{R}m\sigma}$ ($c_{\mathbf{R}m\sigma}$) are the usual fermionic creation (annihilation) operators acting on an electron with spin σ at a site $\mathbf{R}$ in the orbital m. The on-site Coulomb interactions are expressed in terms of two parameters U and J via $U_{mm} = U$, $U_{mm'(\neq m)} = U' = U - 2J$, $J_{mm'} = J$.[44] In our calculations we used values of U in the range of 2–4 eV and J in the range of 0.6–1.2 eV as they are the usual parameters for transition-metal elements.[45–47] Similar values were used to include correlation effects within mean-field GGA + U calculations[48,49] in multiple-decker-type compounds. Note that corrections for a double counting of the interaction within the manifold of orbitals considered only produces an irrelevant constant shift of the chemical potential[50,51] as we are considering a model Hamiltonian with fixed number of electrons.

B. The correlated ferromagnetic state

The total Hamiltonian in Eq. (4) is solved by the variational cluster approach (VCA) method, which is an extension of cluster perturbation theory (CPT).[52–54] In this approach, the original lattice is divided into a set of disconnected clusters and the intercluster hopping terms are treated perturbatively. VCA additionally includes "virtual" single-particle terms to the cluster Hamiltonian, yielding a so-called reference system, and then subtracts these terms perturbatively. The "optimal" value for these variational parameters is determined in the framework of the self-energy functional approach (SFA),[55,56] by requiring that the SFA grand-canonical potential Ω be stationary within this set of variational parameters.

In Fig. 6 we show the choice of the reference system, obtained by disconnecting the multiple-decker nanowire (i.e., the chain of *CP-M* units) into a set of sites connected by the same intra- and intercluster hopping $t^{\mathbf{R}'-\mathbf{R}}_{m',m}$. The electronic

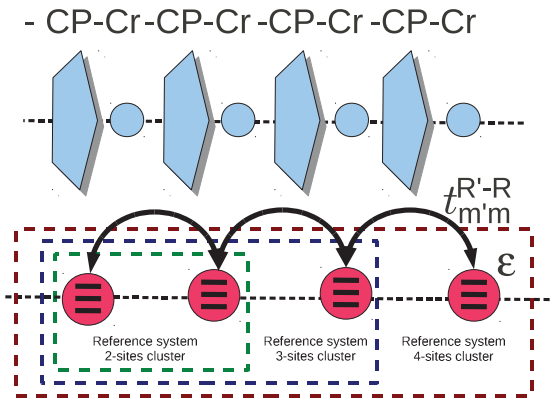

FIG. 6. (Color online) Schematic representation for the model CP-*M* chain. Three different choices for the reference systems are shown: the 2-, 3-, and 4-site clusters. Intra- and intersite couplings are described by the $t^{\mathbf{R}'-\mathbf{R}}_{m',m}$ matrix, with ϵ the on-site energies for the effective d orbitals rotated in the local basis.

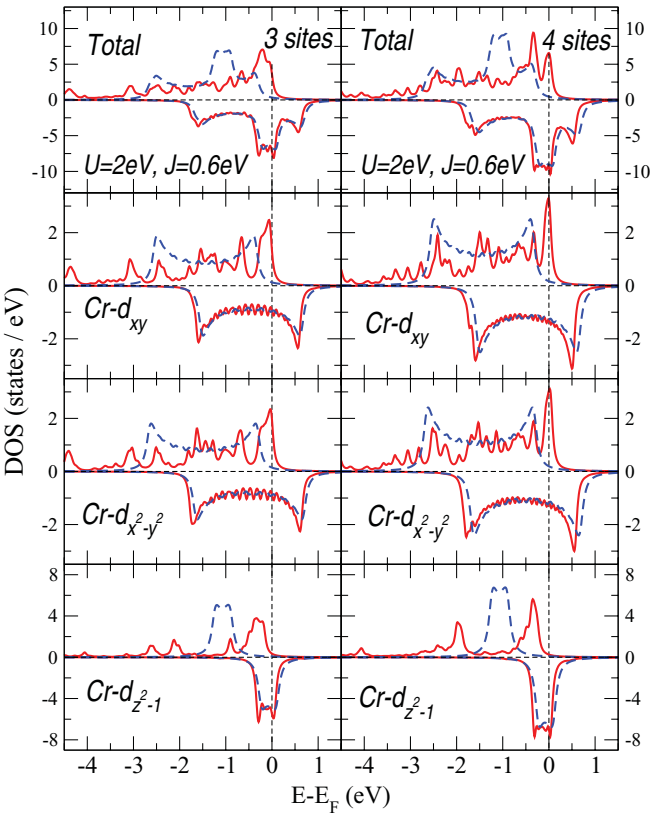

FIG. 7. (Color online) Orbital-resolved densities of states of *CP*-Cr chain for the clusters containing three (left column) and four (right column) sites, and the average Coulomb and exchange interactions are $U = 2$ eV and $J = 0.6$ eV. At the noninteracting level (dashed blue line) a half-metallic solution is obtained, while in the presence of interaction (solid red line) the majority spin gap is closed and a metallic solution is obtained.

states connected to the *CP* rings and some of the lower and higher d energies were integrated out so that the electronic structure around the Fermi level is described by the low-energy Hamiltonian Eq. (4) formed with the three active effective orbitals.

Our finite-size scaling analysis has been performed for the fixed values of $U = 2$ eV and $J = 0.6$ eV parameters for the different clusters of two, three, and four sites. The results indicate that with larger cluster size, convergence and optimization of the VCA grand potential is still easily achieved. In particular, the self-consistent solutions for the grand potential, in the case of three- and four-site clusters, provides similar occupations to the noninteracting case. The noninteracting results were obtained by self-consistent calculations of the grand potential in which the exchange splitting has been considered as a variational parameter. For the four-site cluster, a total magnetic moment of 1.10 μ_B is obtained within the noninteracting calculation while for the interacting case a value of about 0.95–0.97 μ_B is obtained depending on the strength of average Coulomb parameters (U and J).

In Fig. 7 we show the total and orbital-resolved density of states for the clusters of three and four sites and fixed values $U = 2$ eV, $J = 0.6$ eV. As one can see, the majority spin gap is filled and the normal ferromagnetic ground state is

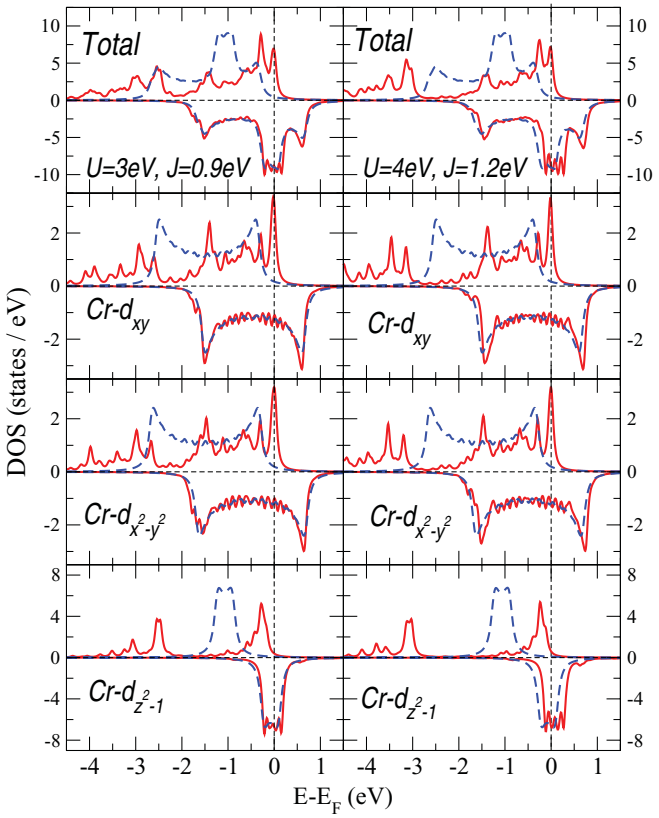

FIG. 8. (Color online) Orbital-resolved densities of states for the four-site cluster (interacting/noninteracting: red solid/blue dashed line) with increasing values of U and J as indicated in the figure.

obtained with a considerable spectral weight just below the Fermi level. In comparing to the noncorrelated calculations (dashed blue line), most significant changes are seen in the majority spin channel for all three orbitals. The majority $z^2 - 1$ orbital is pushed toward the Fermi level and split by electronic correlations; nevertheless it remains completely occupied. The xy and $x^2 - y^2$ orbitals remain almost degenerate and are shifted also toward the Fermi level. In addition they develop a double-peak structure just below Fermi level. Increasing the size of the cluster (see left and right columns of Fig. 7), there is no significant change within the minority spin channel. All essential features of density of states remain unchanged when comparing the results of calculations for three- and four-site clusters. A close look reveals only the scale difference connected of the number of sites considered within the cluster.

In Fig. 8 we present the results for the four-site cluster, for two distinct values of U and J. Increasing the values of U and J, the density-of-states features situated between -4 and -3 eV are further renormalized toward higher binding energies. Within an energy window of ± 1 eV around the Fermi level (see Fig. 9) there is a slight shift of minority spin states toward the Fermi level, while for the majority spins, spectral weight transfer toward the Fermi level is slightly increased for larger U. For the majority electrons, the DOS in the close vicinity of the Fermi level obtained within the many-body calculations shows the presence of some states pinned almost at the Fermi level. The position of these pinned

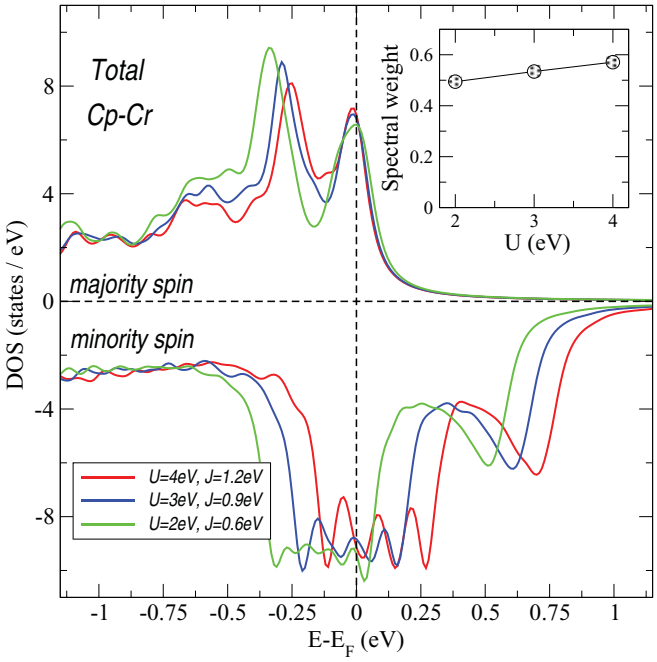

FIG. 9. (Color online) Total density of states for the four-site cluster for different values of U and J parameters. Inset presents the integrated spectral weight of the peak centered at E_F.

states remains practically unchanged for the different U and J parameters, while their spectral weight is slightly increasing with U and J. From the orbital projected densities of states seen in Fig. 7 and Fig. 8 we can identify its composition as being mainly determined by the xy and $x^2 - y^2$ orbitals. Around 0.25 eV below the Fermi level, the peak having mainly a $z^2 - 1$ character is seen to shift toward E_F when U and J increase. In addition spectral weight is transferred toward the peak pinned at the Fermi level. Within the minority spin channel, increasing U/J leads to a visible shift of the $z^2 - 1$ orbital toward and above the Fermi level. The inset of Fig. 9 shows the integrated spectral weight of the states pinned in the close vicinity of the Fermi level. A similar effect has been recently discussed for the ferrimagnet Mn_2VAl in which the local but dynamic electronic correlations captured by dynamical mean-field theory (DMFT)[57] demonstrated the closure of the gap and a very strong depolarization effect. For both these compounds LDA-based DFT calculations predict a half-metallic majority spin gap, but for both materials correlation effects are shown to destroy half metallicity, by creating many-body induced states just below the Fermi level. Because of their position below the Fermi level and their considerable spectral weight, one can expect that these states might be detectable by spin-polarized photoemission, which constitutes an interesting possibility to investigate many-body effects in such organometallic spintronic materials.

V. CONCLUSION

In this work we studied the electronic structure and magnetic properties of a series of metallocene multiple-decker sandwich nanowires with the formula $(C_5H_5)_2M_2$, where $M =$ Ti to Ni. Our results show that a broad variety of electronic and magnetic properties are predicted in these wires

(i.e., insulator, metallic, half metallic). Based on the results of the binding energies, we show that all the structures are energetically stable. We demonstrate that physical properties of the multiple-decker nanowires are determined by structural relaxation. Depending on the transition-metal element we found regular alternations of the geometric parameters such as bond lengths and cell length that determine the magnetic properties of $(C_5H_5)_2M_2$ systems. Accordingly we found that *CP*-Co is an antiferromagnetic insulator with a large gap of about 1.5 eV. The Mn moment's reduction to zero in *CP*-Mn and the considerable turn-up of the V moment in *CP*-V is obtained. For the *CP*-V and *CP*-Ti both ferromagnetic and antiferromagnetic solutions are possible which allows us to estimate the exchange couplings between the V-V and Ti-Ti atoms. These are of magnitude $J_V = 0.34$ eV ≈ 3945 K and $J_{Ti} = 0.17$ eV ≈ 1973 K and the corresponding ground state in these cases is metallic ferromagnetic and antiferromagnetic, respectively. In all calculations the *CP* rings carry a very small induced magnetic moment that contributes to the stabilization of the structure and the transmission of the magnetic interactions through the wire. For the Fe-based and Cr-based sandwiches we found within the DFT-GGA calculations stable half-metallic solutions.

For the *CP*-Cr half-metallic wire we have constructed a low-energy Hamiltonian by downfolding all orbitals except Cr-3*d* (xy, $x^2 - y^2$, $z^2 - 1$) orbitals which provides an effective low-energy model. This simplified model-Hamiltonian is used to investigate correlation effects in the half-metallic ground state. We have solved the three-band Hubbard Hamiltonian within the variational cluster approach. The main effects determined by electronic interactions are as follows: (i) Within the minority channel (spin down) the $z^2 - 1$ orbital is less occupied and more itinerant, while the other minority spin orbitals do not suffer significant change; (ii) for the majority electrons (spin-up channel) the many-body states of xy and $x^2 - y^2$ origin are pinned within the half-metallic gap just below the Fermi level. Their position is practically unchanged for different values of U and J, in contrast to the occupied $z^2 - 1$ orbitals that shift toward the Fermi level with increasing U. The overall conclusion is that the majority spin half-metallic ground state is not robust against the presence of local Coulomb correlations, and a correlated ferromagnetic ground state is obtained in which the majority spin gap is closed by many-body induced states.

ACKNOWLEDGMENTS

We thank I. Leonov for useful discussions. The calculations were performed in the Datacenter of NIRDIMT. C.M. acknowledges the financial support offered by the Augsburg Center for Innovative Technologies (ACIT), University of Augsburg, Germany.

[1] I. Zutic, J. Fabian, and S. D. Sarma, Rev. Mod. Phys. **76**, 323 (2004).
[2] G. Binasch, P. Grünberg, F. Saurenbach, and W. Zinn, Phys. Rev. B **39**, 4828 (1989).
[3] M. N. Baibich, J. M. Broto, A. Fert, F. Nguyen Van Dau, F. Petroff, P. Etienne, G. Creuzet, A. Friederich, and J. Chazelas, Phys. Rev. Lett. **61**, 2472 (1988).
[4] P. Bruno, Phys. Rev. B **52**, 411 (1995).
[5] R. A. de Groot, F. M. Mueller, P. G. van Engen, and K. H. J. Buschow, Phys. Rev. Lett. **50**, 2024 (1983).
[6] M. I. Katsnelson, V. Y. Irkhin, L. Chioncel, A. I. Lichtenstein, and R. A. de Groot, Rev. Mod. Phys. **80**, 315 (2008).
[7] V. V. Maslyuk, A. Bagrets, V. Meded, A. Arnold, F. Evers, M. Brandbyge, T. Bredow, and I. Mertig, Phys. Rev. Lett. **97**, 097201 (2006).
[8] L. Zhou, S.-W. Yang, M.-F. Ng, M. B. Sullivan, V. B. C. Tan, and L. Shen, J. Am. Chem. Soc. **130**, 4023 (2008).
[9] R. Leitsmann, F. Küwen, C. Roödl, C. Panse, and F. Bechstedt, J. Chem. Theory Comput. **6**, 353 (2010).
[10] E. Durgun, D. Çakır, N. Akman, and S. Ciraci, Phys. Rev. Lett. **99**, 256806 (2007).
[11] S. Sanvito and A. R. Rocha, J. Comput. Theor. Nanosci. **3**, 624 (2006).
[12] K. Tsukagoshi, B. W. Alphenaar, and H. Ago, Nature Phys. **401**, 572 (1999).
[13] J. M. Kikkawa and D. D. Awschalom, Nature Phys. **397**, 139 (1999).
[14] Z. H. Xiong, D. Wu, Z. V. Vardeny, and J. Shi, Nature Phys. **427**, 821 (2004).
[15] A. Haaland, Inorg. Nucl. Chem. Lett. **15**, 267 (1979).
[16] E. Gard, A. Haaland, D. P. Novak, and R. Seip, J. Organomet. Chem. **88**, 181 (1975).
[17] A. Haaland, Acc. Chem. Res. **12**, 415 (1979).
[18] A. K. Hedberg, L. Hedberg, and K. Hedberg, J. Chem. Phys. **63**, 1262 (1975).
[19] A. Almenningen, E. Gard, A. Haaland, and J. Brunvoll, J. Organomet. Chem. **107**, 273 (1976).
[20] Z.-F. Xu, Y. Xie, W.-L. Feng, and H. F. Schaefer, J. Phys. Chem. A **107**, 2716 (2003).
[21] A. Salzer and H. Werner, Angew. Chem., Int. Ed. Engl. **11**, 930 (1972).
[22] S. M. Schildcrout, J. Am. Chem. Soc. **95**, 3846 (1973).
[23] S. Nagao, A. Kato, A. Nakajima, and K. Kaya, J. Am. Chem. Soc. **122**, 4221 (2000).
[24] S. Coriani, A. Haaland, and P. Jorgensen, Chem. Phys. Chem. **7**, 245 (2006).
[25] L. Wang, Z. Cai, J. Wang, J. Lu, G. Luo, L. Lai, J. Zhou, R. Qin, Z. Gao, D. Yu, G. Li, W. N. Mei, and S. Sanvito, Nano Lett. **8**, 3640 (2008).
[26] M. Koleini, M. Paulsson, and M. Brandbyge, Phys. Rev. Lett. **98**, 197202 (2007).
[27] T. Kurikawa, H. Takeda, M. Hirano, K. Judai, T. Arita, S. Nagao, A. Nakajima, and K. Kaya, Organometallics **18**, 1430 (1999).
[28] K. Miyajima, K. Muraoka, M. Hashimoto, T. Yasuike, S. Yabushita, A. Nakajima, and K. Kaya, J. Phys. Chem. A **106**, 10777 (2002).
[29] J. M. Soler, E. Artacho, J. D. Gale, A. García, J. Junquera, and P. Ordejón, J. Phys. Condens. Matter **14**, 2745 (2002).
[30] J. P. Perdew, K. Burke, and M. Ernzerhof, Phys. Rev. Lett. **77**, 3865 (1996).
[31] L. Hedberg and K. Hedberg, J. Chem. Phys. **53**, 1228 (1970).
[32] A. Haaland and L. E. Nillson, Acta Chem. Scand. **22**, 2653 (1968).
[33] A. Haaland, Top. Curr. Chem. **53**, 1 (1975).

[34]S. I. Troyanov, H. Antropousova, and K. Mach, J. Organomet. Chem. **427**, 49 (1992).
[35]L. Chioncel, M. I. Katsnelson, R. A. de Groot, and A. I. Lichtenstein, Phys. Rev. B **68**, 144425 (2003).
[36]H. Allmaier, L. Chioncel, E. Arrigoni, M. I. Katsnelson, and A. I. Lichtenstein, J. Opt. Adv. Mat. **10**, 1671 (2008).
[37]H. Allmaier, L. Chioncel, E. Arrigoni, M. I. Katsnelson, and A. I. Lichtenstein, Phys. Rev. B **81**, 054422 (2010).
[38]A. Yamasaki, L. Chioncel, A. I. Lichtenstein, and O. K. Andersen, Phys. Rev. B **74**, 024419 (2006).
[39]H. Allmaier, L. Chioncel, and E. Arrigoni, Phys. Rev. B **79**, 235126 (2009).
[40]Y. X. Yao, C. Z. Wang, G. P. Zhang, M. Ji, and K. M. Ho, J. Phys. Condens. Matter **21**, 235501 (2009).
[41]Y. X. Yao, C. Z. Wang, and K. M. Ho, Phys. Rev. B **83**, 245139 (2011).
[42]O. K. Andersen and T. Saha-Dasgupta, Phys. Rev. B **62**, R16219 (2000).
[43]E. Zurek, O. Jepsen, and O. K. Andersen, Chem. Phys. Chem. **6**, 1934 (2005).
[44]A. I. Lichtenstein and M. I. Katsnelson, Phys. Rev. B **57**, 6884 (1998).
[45]J. Minar, H. Ebert, C. De Nadai, N. B. Brookes, F. Venturini, G. Ghiringhelli, L. Chioncel, M. I. Katsnelson, and A. I. Lichtenstein, Phys. Rev. Lett. **95**, 166401 (2005).
[46]J. Braun, J. Minár, H. Ebert, M. I. Katsnelson, and A. I. Lichtenstein, Phys. Rev. Lett. **97**, 227601 (2006).
[47]S. Chadov, J. Minár, H. Ebert, A. Perlov, L. Chioncel, M. I. Katsnelson, and A. I. Lichtenstein, Phys. Rev. B **74**, 140411 (2006).
[48]H. Weng, T. Ozaki, and K. Terakura, J. Phys. Soc. Jpn. **77**, 064301 (2008).
[49]H. Weng, T. Ozaki, and K. Terakura, Phys. Rev. B **79**, 235118 (2009).
[50]O. Parcollet, G. Biroli, and G. Kotliar, Phys. Rev. Lett. **92**, 226402 (2004).
[51]A. G. Petukhov, I. I. Mazin, L. Chioncel, and A. I. Lichtenstein, Phys. Rev. B **67**, 153106 (2003).
[52]C. Gros and R. Valenti, Phys. Rev. B **48**, 418 (1993).
[53]D. Sénéchal, D. Perez, and M. Pioro-Ladriere, Phys. Rev. Lett. **84**, 522 (2000).
[54]S. G. Ovchinnikov and I. S. Sandalov, Physica C **161**, 607 (1989).
[55]M. Potthoff, Eur. Phys. J. B **32**, 429 (2003).
[56]M. Potthoff, Eur. Phys. J. B **36**, 335 (2003).
[57]L. Chioncel, E. Arrigoni, M. I. Katsnelson, and A. I. Lichtenstein, Phys. Rev. B **79**, 125123 (2009).